Submitted to Physical Review

LBL-374
Preprint
c.1

PHOTON SPECTRA FROM RADIATIVE ABSORPTION OF PIONS IN NUCLEI

J. A. Bistirlich, K. M. Crowe, A. S. L. Parsons,
P. Skarek, and P. Truöl

September 1971

AEC Contract No. W-7405-eng-48

For Reference

Not to be taken from this room

LBL-374
c.1

DISCLAIMER

This document was prepared as an account of work sponsored by the United States Government. While this document is believed to contain correct information, neither the United States Government nor any agency thereof, nor the Regents of the University of California, nor any of their employees, makes any warranty, express or implied, or assumes any legal responsibility for the accuracy, completeness, or usefulness of any information, apparatus, product, or process disclosed, or represents that its use would not infringe privately owned rights. Reference herein to any specific commercial product, process, or service by its trade name, trademark, manufacturer, or otherwise, does not necessarily constitute or imply its endorsement, recommendation, or favoring by the United States Government or any agency thereof, or the Regents of the University of California. The views and opinions of authors expressed herein do not necessarily state or reflect those of the United States Government or any agency thereof or the Regents of the University of California.

0 0 0 0 3 7 0 1 8 1 2

PHOTON SPECTRA FROM RADIATIVE ABSORPTION OF PIONS IN NUCLEI*

J. A. Bistirlich, K. M. Crowe, A. S. L. Parsons†, P. Skarek††, and P. Truöl‡

Lawrence Berkeley Laboratory
University of California
Berkeley, California 94720

September 1971

ABSTRACT

The photon spectra following capture of stopped pions in ^{4}He, ^{12}C, ^{16}O, ^{24}Mg, and ^{40}Ca have been measured for photon energies between 50 and 160 MeV. A pair spectrometer was used and a resolution of 2.0 MeV FWHM was achieved. On the basis of several thousand events for each spectrum, we observe collective excitation in the residual nucleus for capture on ^{4}He, ^{12}C, and ^{16}O. Such excitation is predicted theoretically, and in some cases the detailed comparison with the data is good. For ^{24}Mg and ^{40}Ca, no significant structure is seen. In addition, the transition rates to particle-stable states in ^{16}O and ^{12}C have been measured. A continuum background consistent with a direct reaction mechanism is also observed for all the elements studied except for ^{4}He. Results for the pion capture rates in CH_2 and H_2O are given.

0 0 0 0 3 7 0 1 6 1 3

I. INTRODUCTION

Using a pair spectrometer we have measured the photon energy spectrum between 50 and 160 MeV, arising from the radiative capture of stopped pions in various nuclei: ^{4}He, ^{12}C, ^{16}O, ^{24}Mg, and ^{40}Ca. Although data from ^{4}He and ^{12}C have already been published,[1,2] we present them with the new data for completeness. Discussion of these two elements will be confined mainly to new information.

In this section we discuss the theoretical and experimental background to the radiative capture process. In Section II we describe the experimental technique; and in Section III we discuss our results for each element, together with earlier experimental work for that element and relevant theoretical predictions.

The process under study, expressed generally, is

$$\pi^- + N(A, Z) \rightarrow N^*(A, Z-1) + \gamma. \qquad (1)$$

For the lightest nuclei, e.g, ^{4}He, the pion will be captured mainly from a 1s Bohr orbit; as the mass of the nucleus increases, capture from 2p and higher orbits predominates (for example, about 80% of pions are captured from 2p orbits in ^{12}C). Radiative capture is typically ~ 2% of the total capture rate. Much of the interest in this process derives from its close similarity with negative muon capture,

$$\mu^- + N(A, Z) \rightarrow N^*(A, Z-1) + \nu_\mu, \qquad (2)$$

in which the capture is always from 1s orbits and accounts for essentially the whole rate. The analogy has been extensively discussed in theoretical terms in the recent literature; only the more prominent features of it will be mentioned here.

The most obvious analogy between reactions (1) and (2) arises

from the closeness of the masses of the participating particles, so that the momentum transfers are of the same order--0.92 m^2_π for (1) and 0.52 m^2_π for (2). A more subtle and far-reaching analogy comes from the fact that the matrix element for pion capture, reaction (1), leading to a particular final state can be expressed in terms of the same axial vector and pseudoscalar nuclear form-factors (f_A and f_p) as appear in the muon capture matrix element to the same final state: muon capture has additional vector terms. This equality has been derived using both the impulse approximation and PCAC.[3] However, the impulse approximation has been compared with the PCAC approach for ^{6}Li,[4] and significant model-dependent corrections to the latter approach are required. Given that the vector terms in muon capture can be derived from inelastic electron scattering data (using CVC), the rates for (1) and (2) can be related. It should be emphasized that this is only true for capture from 1s orbits. Since with present experimental techniques one cannot isolate the contributions to the capture rates from different orbits, this means that the comparison has been made only for the lightest nuclei, and even then significant corrections are required for p-state capture. There has been considerable theoretical discussion on ^{3}He,[5] ^{4}He,[6] and ^{6}Li.[4] Rescattering corrections to the pion capture rate are also of importance and become more so the heavier the nucleus (e.g. a 40% correction is required for ^{16}O).[7]

An experimental test of the above analogy has been performed for ^{6}Li by Deutsch et al.[8] Using activation techniques, they measured the branching ratio to the ground state in the residual nucleus for muon capture and radiative pion capture; the observed agreement

between the two branching ratios may be taken as being consistent with the above analogy.

Perhaps of greater interest than the reaction mechanism itself is the possibility, in reaction (1), of observing excited states in the residual nucleus that are inaccessible by other means.[9] Specifically, collective nuclear excitations are expected as final states of both reactions (1) and (2), but are only observable directly in (1). These states are the $I_3 = -1$ components of the collective states observed in photoexcitation or inelastic electron scattering on the parent nucleus.

In order to explain the total muon capture rate in ^{16}O, it was originally proposed that collective states were excited in process (2).[10] Further experimental evidence for such excitation has been meager and necessarily indirect. The experimental problem for this reaction is that only the decay products of the residual nucleus can be detected. These have been either the <u>secondary</u> neutrons from the decay of the collective states (their energy spectrum has been derived from recoil proton spectra),[11, 12] or the <u>tertiary</u> low-energy gamma rays from the decay of the products of the collective state decay; Kaplan et al.[13] have, for instance, studied the spectrum of low-energy gamma rays arising from the sequence: $\mu^- + {}^{16}O \rightarrow {}^{16}N^* + \nu_\mu$, ${}^{16}N^* \rightarrow {}^{15}N^* + n$, ${}^{15}N^* \rightarrow {}^{15}N(g.s.)$. Both methods have yielded data which can be interpreted as evidence for collective state excitation.

Radiative pion capture offers two experimental advantages. For neutron spectroscopy, a time-of-flight "start" signal is provided by the promptly captured pions. The photon energy spectrum may be measured, using a pair spectrometer, with sufficient resolution to

resolve resonant peaks in the residual spectrum, as will be demonstrated by our results. This photon spectrum is the most direct way of observing the collective states; the neutron spectrum yields additional information on their decay properties. Neutron spectra have been measured by two groups.[14, 15] Although these measurements show evidence of structure, the data are in general lacking in statistics. Specific examples are referred to in Section III. Davies et al.[16] have measured the photon spectrum from radiative pion capture on several elements using a sodium iodide crystal. There was insufficient resolution to allow resonances to be observed, but the data allowed the total branching ratio (typically about 2%) to be established.

It has been pointed out[17, 18] that it may be possible to exploit the differences between μ-capture and radiative pion capture. First, since radiative pion capture occurs from higher Bohr orbits than the 1s for all but the lightest elements, this opens up the possibility of exciting collective quadrupole states. Murphy et al.[18] have shown, for instance, that for 2p capture in ^{16}O, transitions to quadrupole states are the dominant ones. It would appear therefore that radiative pion capture may allow the observation of these hitherto unobserved states. Second, since the radiative pion capture matrix element contains only the axial vector term, it will lead to fewer states than muon capture; thus it is a preferable mechanism for the initial exploration of the spectrum of collective states.

II. EXPERIMENT

A. Apparatus

The experiment was carried out at the Berkeley 184-in. cyclotron with the setup shown in Fig. 1. A beam of 80-MeV negative pions was extracted from an internal target. After passing through a quadrupole doublet, a bending magnet, and another doublet, the beam was focussed onto various targets. Before the target, the pions were degraded to optimize the stopping rate in the target (3 to 5×10^5 pions/sec^{-1}). A pion brought to rest in the target was identified by a coincidence signal from counters π_1, π_2, and π_3 in front of the target in anticoincidence with any of the counters π_{Si} behind the target (between 1 and 4 in number depending on the target). Two time-of-flight counters, one upstream in front of the bending magnet and one downstream in front of the degrader, were employed to measure the electron and the muon contamination of the beam. These amounted to 10.7% electrons and 1.7% muons without degrader, and 14.6% and 5.6% with degrader.

For the detection of the γ rays a large solid angle pair spectrometer was constructed. It was located at 90 deg to the direction of the incoming π^-. The spectrometer consisted of two 46 cm $\times$ 91 cm C-magnets combined with a common pole tip to give an analyzing area 218 cm in length with a 33-cm gap. The maximum possible field in this configuration was 10 kG, the normal field during the experiment being 8 kG. It was measured in 2.5-cm steps to an accuracy of 0.2% throughout the volume using a "rapid mapper". The γ rays were converted into electron-positron pairs in a 3% radiation length of gold foil (0.011 cm) mounted on a thin styrofoam backing

and placed at 109 cm from the target. The conversion probability for our photon energies was 2.3%. The field chosen was sufficient for a 180-deg bend of the electrons and positrons up to momenta of 110 MeV/c, and yielded maximum efficiency for photon energies around 120 MeV. The directions of electron-positron pairs at entry and exit of the spectrometer were measured using six arrays of four-gap spark chambers (shown in Fig. 1) arranged in two rows parallel to the magnet, with the converter foil in between. To minimize multiple scattering and energy loss of the particles, the spark chambers were constructed of low-mass material (20 mg per gap). The gaps were made of 0.0012-cm aluminum foil on a fluorine-free styrofoam backing.[19] The inside of the spectrometer magnet was filled with a helium bag to reduce multiple scattering.

The tracks were recorded optically. Mirrors on top of the chambers within the gap of the magnet coils and on the sides allowed a two-dimensional view with a camera mounted on a stand approximately 4 m above the two spectrometer magnets.

A lead shielding wall between the beam line and the spark chambers reduced the background in the spectrometer. To eliminate charged particles entering the magnet, an aperture (29 cm × 14 cm) in the wall was covered with a counter in anticoincidence with the beam trigger. Six pairs of counters covered the full length of the spark chambers; a coincidence signal from any two of them that were nonadjacent but <u>only</u> from two was regarded as a good electron-positron pair leaving the magnet, and was combined with beam-signal to trigger the spark chambers. Inspection of the pictures showed that only 20% of all trigger were due to a genuine pair. The main source

of background events was γ rays converting in the side of the collimating aperture, in the lead shielding wall, and in other material besides the converter foil. These events in general showed only one electron or positron trajectory, or showed a pair with tracks not originating in the converter. They could easily be separated from the real events which have a very distinct signature. The total number of events collected was 680×10^3 (of which 120×10^3 were good pairs) for the following targets: oxygen 110(20), magnesium 57(10), water 12(2), lithium 21(3), calcium 54(10), carbon 100(20), CH_2 49(10), hydrogen 147(30), and helium 130(16) (all in 10^3).

B. Analysis.

The spark chamber pictures were scanned by hand with a semi-automatic coordinate recorder (TRAMP). For each event, the center and the angle of inclination of the six tracks in top and side views and five fiducial marks were measured. For the first five events of each roll of 500 events, the total of 19 fiducial marks were measured. The accuracy of reconstruction achieved by this method was ±0.3 cm. In the analysis, an iterative tracking procedure was used to obtain the best-fit momenta to the coordinate and angles of the electron and positron. The sum of the two momenta directly gives the γ energy, apart from energy-loss corrections.

In order to check the resolution and efficiency of the spectrometer, we performed a calibration experiment using a liquid hydrogen target The reaction $\pi^- p \rightarrow n\gamma$ with pions at rest gives a monochromatic γ ray of 129.4 MeV. This provides a measurement of the

resolution as well as a calibration of the energy scale independent of the field measurement. The spectrum of γ rays produced in the charge-exchange reaction ($\pi^- p \rightarrow n\pi^0 \rightarrow n\gamma\gamma$) serves as a check on the low-energy end of the efficiency curve. The energy spectrum from mesonic capture is flat between 55 and 83 MeV. The measured spectrum is shown in Fig. 2. The resolution (ΔE) for the 129.4-MeV photon is 2.0 MeV FWHM, with the usual long low-energy tail. There are several contributions to this resolution (all evaluated at 130 MeV).

a) Energy straggling in the converter and the spark chambers; $\Delta E = 0.8$ MeV.

b) Uncertainties in the magnetic field map between different positions of 0.2%: $\Delta E = 0.3$ MeV.

c) Multiple scattering in the converter and the spark chamber, resulting in an angle uncertainty of 2 deg: $\Delta E = 0.1$ MeV.

d) Spatial resolution of 0.3 cm: $\Delta E = 1.6$ MeV.

e) Uncertainty in the absolute field value between different runs 0.25%: $\Delta E = 0.4$ MeV.

The major contribution arises from reconstruction errors, which are introduced in the scanning process.

In order to calculate the efficiency of the spectrometer and to estimate the different contributions to the resolution, an extensive Monte Carlo calculation was performed. This simulation included, besides the exact geometry, the measured magnetic field, theoretical expressions for the pair-production probability, energy loss and multiple scattering of the electron-positron pair in the converter and the subsequent material transversed, and additional uncertainty in track location due to inaccuracies in the measuring procedures.

Events generated in this fashion were subjected to the same analysis program as the measured events. The efficiency of the spectrometer as a function of the energy is also given in Fig. 3. This efficiency $\eta_\gamma (E_\gamma)$ contains the solid angle, the conversion and detection efficiency, and a factor $1/4\pi$. The decrease in efficiency towards lower energies is due to the following factors:

1. Electrons or positrons, below 15 MeV that curl up in the spectrometer and do not trigger the exit counters.
2. The requirement that two nonadjacent counters must report, which was necessary in order to reduce the rate of bad triggers.

A comparison of the observed and the calculated electron and positron energy distribution indicated an apparent drop in efficiency of the spark chamber for energies below 25 MeV. When this effect was included in the Monte Carlo calculation, the Panofsky ratio (the intensity ratio between photons from mesonic and radiative capture) determined from the hydrogen spectrum was 1.44 ± 0.16, in agreement with the presently accepted value of 1.53 ± 0.02 .[20]

The absolute efficiency can be checked when the yield of photons from radiative capture per stopped π is calculated. The theoretical value is $(39.5 \pm 0.03)\%$, in complete agreement with the experimental value of $(41.9 \pm 3.3)\%$. The latter was obtained in the following way

$$f = \frac{\sigma(\pi^- p \rightarrow n\gamma)}{\sigma(\pi^- p \rightarrow n\gamma) + \sigma(\pi^- p \rightarrow n\pi^0)} = \frac{N_\gamma (129.4 \text{ MeV})}{N_\pi^* \, \eta_\gamma} .$$

Here $\eta_\gamma = (2.18 \pm 0.11) \times 10^{-5}$ and N_γ is the number of γ rays in the spectrum, which has to be corrected for the conversion and absorption of the photons in the target, the target walls, and the counters in

front of the converter. In the case of hydrogen, where we used a 120 liter liquid-hydrogen dewar as a target, these corrections amount to 11.6%. A further correction arises from pions being captured in the target walls. This effect, which was almost negligible, was measured with an empty target and subtracted from the raw spectrum. The number of pions stopped in the target (N_π) is determined in two ways: First, by subtracting the number of stopped pions for full and empty targets, normalizing both to the same number of incoming π; this accounts not only for those pions stopping in the walls of the target but also for those that do not stop in the target but yet do not register in the anticounter behind the target as a result of geometric or electronic inefficiencies. The second way is by differentiating a range curve for the incoming pions for a total mass equivalent to the hydrogen in the target at the corresponding range. Both methods agree within 2%. A further small correction has to be applied for the number of muons and electrons stopping. From the comparison of the hydrogen rates, we are confident that our absolute rates for all targets can be determined to about 15% using the same procedure. An exception is oxygen.

We now discuss each target in turn. The ingredients for the calculation of the experimental capture rates are given in Table I.

1. Helium

The energy spectrum of photons from radiative pion capture in ^{4}He is shown in Fig. 4. Here we have used a 120 liter liquid-helium container as a target. Radiative pion capture in the wall materials and the target were equally probable. Therefore the target-out rate was 30% of the target-in rate. Figure 4(b) shows the resulting spectrum.

2. Carbon

The carbon target used in determining pion capture in ^{12}C (Fig. 5) was a 2.5-cm slice of graphite placed at 45 deg to the beam. Due to the thickness of the target, the experimental spectrum also had to be corrected for interactions occurring for pions in flight. We have measured the γ spectrum for (38 ± 6) MeV pions to assure ourselves that no structure is seen for higher pion energies. In fact, the experimental spectrum can be fitted with a pure $^{11}B+n+\gamma$ phase-space curve. We have normalized the in-flight spectrum to events with photon energies greater than 130 MeV and subtracted it from the raw spectrum. This correction amounts to 20% for carbon; in the hydrogen case, it can be neglected. Subtracted spectrum is shown in Fig. 5b.

3. Oxygen

In the oxygen case (Fig. 6), a 34-cm diameter liquid-oxygen container was used as a target. In order to assure that the majority of the pions stopped near the center of the target and not in the thick steel walls of the container, the undegraded beam was allowed to hit the target. This leads to the complication that a large number of events due to capture occurring in flight had to be accepted. This problem was overcome by reconstructing from the spark-chamber tracks the origin of the γ ray in the target along the beam direction, and eliminating those events which originated in regions with an average range of less than 80% of the range corresponding to the central momentum of the beam. The raw and the subtracted spectra are displayed in Figs. 6(a) and 6(c) respectively. With the uncertainty in

reconstructing the origin of the γ ray ($\pm$ 1.8 cm) and the large error in evaluating the corresponding number of stopped pions, our absolute normalization error is 20% in this case. The total rate measured agrees very well with the one obtained from a smaller sample of data taken with a water target, in which the correction for in-flight capture is less important and the number of stopped pions can be evaluated with greater confidence (see Appendix).

4. Magnesium

To obtain the spectrum for ^{24}Mg we used as a target natural magnesium powder (4.1 g/cm^2) in a thin aluminum container placed at 33 deg to the beam direction.

5. Calcium

For the ^{40}Ca spectrum (Fig. 8), 7.3 g/cm^2 of natural calcium-metal was used as a target. For calcium as well as magnesium the in-flight background was not measured, so we used the in-flight spectrum from oxygen for this correction. This is justified, since the identity of the in-flight spectra from carbon and oxygen suggests that the shape is independent of the target nucleus.

To evaluate the total radiative capture rate, including the parts of the spectrum with γ energies below 50 MeV, an assumption concerning the shape of the spectrum at lower energies is needed. Since the low-energy spectrum is completely due to the direct mechanism with emission of a neutron, and since the pole model (see below) describes the slope for energies between 50 and 90 MeV very well, we can compute the amount of the missing spectrum. For lower photon energies, the pole model and pure phase space become very similar. Typically,

the missing part of the spectrum amounts to less than 15% of the total spectrum.

III. DISCUSSION

In this section we discuss our results for each element in turn; however, there are some general comments that are relevant to all on several elements. First, the spectra of all elements display a "continuum" component, although in the case of helium the whole spectrum can be accounted for by broad-resonance contributions. There are three models, all rather naive, which may be used to attempt to fit this continuum.

In the Fermi gas model, one assumes the fundamental radiative interaction of a pion with a proton in the nucleus ($\pi^- p \rightarrow n\gamma$) in which the proton energy distribution is that of a Fermi gas; no final-state interaction is assumed. In the earlier work by Davies et al.[16] using a sodium iodide crystal (which gives relatively poor energy resolution), the Fermi gas model was shown to provide a reasonable description of the observed spectra. However, with the better resolution of our instrument we have shown that the model gives much too sharp a peak, with no contribution to the low-energy part of the spectrum.[21]

At the other extreme, a phase-space calculation assumes that the rest energy of the pion is shared among the photon, one neutron, and the residual nucleus in its ground state. Again, the predicted photon energy spectrum gives poor agreement for all elements (see for instance ^{12}C in Ref. 21), in this case because it is too flat.

The third model is the pole model suggested by Dakhno and Prokoshkin,[22] in which one assumes the exchange of a single proton.

The Q-value at the nucleus vertex is a free parameter, and we have assumed the residual nucleus to be in its ground state. Varying the Q-value produces an overall shift in the energy scale of the final spectrum (see Ref. 22). As for the previous models, normalization is arbitrary. For ^{12}C the pole model fits the continuum shape well, while for the heavier elements the fit become less good (see below). It is clear that this model is over-simplified in that both the initial state of the proton and the final-state interactions (as well as other possible exchanges) are ignored. However, since it fits the continuum better than other available models, we have applied it where necessary.

Our second general comment concerns the question of probability of capture from particular initial pion orbits. This is relevant to ^{12}C and ^{16}O, for which predictions have been made regarding the capture rates from particular orbits--namely, from the 1s and 2p orbits. In general, these dominate the total capture rate.

The quantity we measure is the branching ratio (R) of radiative to total capture for all orbits, either for the whole spectrum or for some part of it, e.g. the resonant peak. We wish to relate the measured quantity to those predicted. We have

$$R = \left(\Lambda_{1s}^{rad}/\Lambda_{1s}^{tot}\right)\omega_{1s} + \left(\Lambda_{2p}^{rad}/\Lambda_{2p}^{tot}\right)\omega_{2p}$$

where the quantities Λ_{1s}^{rad} and Λ_{2p}^{rad} are the theoretically predicted widths for radiative capture, and ω_{1s} and ω_{2p} are relative probabilities for capture from 1s and 2p orbits, respectively. The total capture rates and capture probabilities for 1s and 2p are derived from pionic X-ray data as follows (the treatment of higher orbits is neglected)

$$\Lambda_{1s}^{tot} = \hbar\, \Gamma_{1s}^{tot} = \hbar\, \Gamma_{2p \to 1s} \quad \text{(measured)},$$

taking the width of the $2p \to 1s$ pionic line as being entirely due to the 1s level width.

$$\Lambda_{2p}^{tot} = \hbar\, \Gamma_{2p}^{tot} = \Lambda_{2p \to 1s}^{e.m.} \; \frac{P(2p) - Y(2p \to 1s)}{Y(2p \to 1s)},$$

where $\Lambda_{2p \to 1s}^{e.m.}$ is the calculated electromagnetic rate for the $2p \to 1s$ transition $P(2p)$ is the calculated population of the 2p level, and $Y(2p \to 1s)$ is the measured $2p \to 1s$ yield.[23] The capture probabilities ω_{1s} and ω_{2p} are given by $\omega_{1s} = \frac{Y(2p \to 1s)}{P(2p)}$ and $\omega_{2p} = \frac{P(2p) - Y(2p \to 1s)}{P(2p)}$. Here we assume that both the total and radiative absorption probabilities from s and p orbits with higher principal quantum numbers are the same as for $2p \to 1s$. Some authors[24] have disputed this assumption. Clearly only detailed cascade calculations can resolve the question. [However, we point out that our assumption is approximately valid for ^{6}Li, for which Stapp[25] has presented a capture schedule.]

As mentioned above, the yields and populations are derived from X-ray data. Unfortunately, for the lighter elements and including ^{12}C and ^{16}O, there are some differences between the yields measured by different groups, although the relevant populations calculated by these groups in fact agree. This discrepancy is particularly disturbing since in our treatment the observed branching ratio is proportional to the disputed yield:

$$R = \left[\left(\Lambda_{1s}^{rad} / \hbar\, \Gamma_{2p \to 1s}\right) + \left(\Lambda_{2p}^{rad} / \Lambda_{2p \to 1s}^{e.m.}\right)\right] \times \frac{Y(2p \to 1s)}{P(2p)}.$$

Since we are not in a position to resolve these differences, we have arbitrarily chosen the data of the CERN group for ^{16}O; and for ^{12}C we have taken the mean of the CERN, Virginia, and Berkeley data, which are in agreement. We list in Table II the parameters used in the subsequent calculations. In Table III, the total and partial capture rates for experiment and theory are compared.

A. Helium

There has been no previous experimental work on either muon- or radiative pion-capture in ^{4}He. The residual nucleus in this case is ^{4}H. From both phase-shift analysis of 3N(N, N)3N interactions[26] and from shell-model calculations for excited states in the four-nucleon system. These states are in general wide and overlapping. In our earlier paper we showed that our data are not consistent with phase space or with the pole model, but can be entirely accounted for by assuming excitation of only three of the above states of the ^{4}H system: i.e., 2^-(3.4 MeV) above the $^{3}H+n$ threshold), 1^-(5.1 MeV), and 1^-(7.4 MeV). Indeed, an R-matrix calculation[1] reproduced both the spectral shape and the absolute rate observed in the experiment [see Fig. 4(b)]. Note, however, that this comparison assumed capture entirely from the 1s orbit, although 2p capture has recently been measured to be about 50% of the total capture rate.[27] In a more detailed study of radiative capture of pions in ^{4}He, Raiche and Werntz[6] have discussed the effect of including 2p capture. However, the 2p contribution to the total radiative rate of $(2.1 \pm 0.7)\%$ is only 0.2 %. The spectral shape is essentially unchanged although the low-energy tail of the 2p capture spectrum falls off faster than for 1s capture.

Within the large errors, the predicted total rate is in agreement with the experimental value. The authors have pointed out that the angular correlation between the photon and the neutron are very dissimilar for 1s and 2p capture, allowing the possibility of measuring the respective radiative-capture rates by means of an $n\gamma$ angular distribution.

B. Carbon

Assuming only giant resonance excitation, Kelly and Überall[17] have made theoretical prediction for the photon and the neutron energy spectrum following radiative pion capture in ^{12}C (from both 1s and 2p orbits): all spectra show several distinct peaks. These predictions have been made using two different models for the giant resonances: that of Lewis and Walecka (positions and amplitudes only)[28] and of Kamimura et al. (positions, amplitudes, and widths).[29]

1. Previous Experiments

The neutron energy spectrum following muon capture has been measured by Plett and Sobotka.[12] After subtracting an "evaporation continuum", they observed a broad peak between 4.0 and 7.0 MeV. This structure is fitted quite well by the theoretical predictions based on the Arima model,[29] if the energy scale of the latter is shifted upwards by 1.5 MeV. However, the predicted rate to collective-state excitations is about 1.6 times the measured rate.

Davies et al.,[16] using a sodium iodide crystal, first established for this element a radiative pion capture branching ratio of $1.6 \pm 1\%$. The neutron spectrum associated with radiative pion capture has been measured by Gotow et al.,[15] and although the statistical accuracy is poor, a peak, interpretable as being due to giant-resonance

excitation, is evident. Hilscher et al.[24] have studied ^{12}B(g.s.) activity from both muon capture and radiative pion capture in ^{12}C. They have derived absolute rates and branching ratios for ^{12}B(g.s.) formation in each case. A discrepancy between these data and our own will be discussed later.

2. Discussion of Data

Our measured spectrum is shown in Fig. 5(b). Peaks above a continuum are observed at 117, 120, and 125 MeV (for precise corrected energies see Table III). The peak at 125 MeV can be associated with production of the ^{12}B ground state; however, a difference of 0.4 MeV exists between the expected and the observed peak position for this state. The CH_2 data indicate that this difference cannot fully be accounted for by uncertainties in the energy scale (Table III). We cannot therefore exclude the possibility of an unresolved transition to the 0.95-MeV state.

For the interpretation of the other two peaks, we need to discuss the continuum. As mentioned previously in this section, the pole model[22] fits the continuum well in those regions where there is no structure (50 to 90 MeV). It has therefore been normalized in this region and is taken to represent the background under the peaks at the higher end of the spectrum. Since in this region the continuum is a rapidly varying function of the photon energy, uncertainties in the amplitudes and in the 117- and 120-MeV peak positions arise from this assumption. Note particularly that a change in Q-value at the nucleus vertex in the pole model shifts the endpoint of the continuum. This uncertainty is not included in the quoted errors (see Table III). In order to determine the parameters of the peaks, we have fitted to the

observed spectrum a function consisting of the pole model together with three independent Breit-Wigner resonances, with the experimental resolution folded in. Figure 5(c) shows the spectrum with the pole model subtracted. The dotted curve in this figure shows the predictions of Kelly and Überall[17] using the Arima model; here the 1s and 2p theoretical spectra have been appropriately weighted and summed and the experimental resolution has been folded in. Note that the model does not attempt to describe ^{12}B (g. s.) production nor does it include quadrupole states. The model requires a shift of about 2 MeV downwards to fit the data; this shift is in close agreement with that deduced from the neutron spectrum from radiative capture experiments of Gotow et al.[15] and from the neutron spectrum from muon capture experiments of Plett and Sobotka.[12] The second model of Lewis and Walecka predicts resonance amplitudes and positions only; these predictions are compared with the observed parameters in Table II. Agreement is reasonable. We also have a slight excess of events above the continuum around 105 MeV, where the model predicts a 1^- state.

In the same table we give our values for the branching ratio to the ^{12}B(g. s.), $(0.092 \pm 0.009)\%$ and the total radiative branching ratio, $(1.92 \pm 0.19)\%$. The latter is in fair agreement with that of Davies et al.,[16] $(1.60 \pm 0.1)\%$, and with the two theoretical predictions: by Delorme and Ericson[3] and Anderson and Eisenberg.[9] It is with regard to the branching ratio to the ^{12}B(g. s) that we are in disagreement with the experimental value of $(0.58 \pm 0.13)\%$ obtained in the activation studies of Hilscher et al.[24] Several points should be noted.

(a) The activation measurment yielded the total rate for production of $^{12}B^*$ particle-stable states that end up in the ground state; for example, the 0.95, 1.67, and 2.62 MeV levels would be included if they were excited. However, examination of our spectrum allows us to reject this as an explanation of the discrepancy. The rate to the 0.95-MeV state would essentially be included in our "ground state" peak. The other two levels, if they were excited with sufficient strength to explain the discrepancy (i.e., with rates about four times that of the ground state), would more than completely fill in the dip observed at 122-MeV photon energy. The particle-unstable states at 117 and 120 MeV clearly cannot decay into the ground state.

(b) Our ^{12}B(g. s.) amplitude determination is essentially free of uncertainties due to the pole-model background substraction. The predicted continuum lies only beneath the particle-unstable states.

(c) The two facts, that our total branching ratio agrees with previous experimental work (as well as with theoretical predictions) and that the hydrogen calibration was satisfactory, essentially exclude the possibility of a normalization error in our work.

(d) A further independent measurement of the branching ratio to the ^{12}B ground state can be obtained through analysis of the spectrum from a CH_2 target (see Appendix). The 129.4-MeV hydrogen line and the 125-MeV carbon structure are both appearing simultaneously, so only the relative probability (f) for capturing pions in hydrogen versus carbon in polyethylene has to be known, in order to determine the desired carbon yield. Since the energies involved are only 4 MeV apart, all other factors such as efficiency, loss due to conversion of photons in the target, etc. cancel. If we fit the part of the CH_2 spectrum

above 122 MeV with two lines folded with our resolution, we obtain a value for the ^{12}B (g. s.) branching ratio of 0.135 ± 0.036)%. This value is close to our quoted value, and still is a factor of 4 away from the value obtained by Hilscher et al. In this calculation we use the average value of the five previous measurements of f (see Appendix), not including our own value. The polyethylene spectrum also results in an independent test of the transition energy; we find the hydrogen line at 129.4 MeV and the carbon line at 124.45 MeV.

(e) It should be mentioned that the total branching ratio for muon capture to ^{12}B(g. s.) obtained by Hilscher et al. is in good agreement with the earlier experimental result.[30] This leaves the possibility of nonradiative backgrounds from ^{12}C(n, p) ^{12}B(g. s.) reactions of secondary neutrons emitted after pion capture. Estimates using measured cross sections indicate, that this process could in fact account for the difference. This possibility was independently suggested by Maguire and Werntz.[31] Their calculation of the capture rate to ^{12}B (g. s.) yielded a value of (0.062 ± 0.018)%. If transitions to the 2^+ state at 0.85 MeV and the 2^- state at 1.67 MeV are included, which we cannot separate experimentally, a value of (0.097 ± 0.030)% is obtained, in excellent agreement with our data. In this calculation the X-ray data of the CERN and Berkeley groups were used, similar to our choice. If the X-ray data by Stapp are used, the rate becomes (0.041 ± 0.012)%. The capture rate is obtained using matrix elements from inelastic electron scattering, β decay, and photo-absorption, and is independent of the use of a specific nuclear model. The large error is predominantly due to the inaccurate X-ray data; the precision of the theoretical rates is 14% for 1s and 9% for 2p.

C. Oxygen

For oxygen, Murphy et al.[18] have evaluated photon and neutron spectra following radiative pion capture, using a generalized Goldhaber-Teller model of the giant resonances. This calculation includes quadrupole states; and though there may be some uncertainty in their position, they are predicted to be the most prominent states excited by 2p orbit capture (which in ^{16}O is the most favored orbit for capture).

1. Previous Experiments

Evseyev[11] and Plett and Sobotka[12] have both obtained the neutron energy spectrum following muon capture in ^{16}O. Although there are some differences in the two sets of data, peaks are observed in qualitative agreement with calculations by Kelly and Überall[17] even though, as in ^{12}C, the theoretical predictions are too high by about a factor 2. Of course, since capture is entirely 1s in this case, no significant quadrupole excitation is expected.

Kaplan et al.[13] have observed low-energy gamma-ray spectra (following muon capture in ^{16}O) which are interpreted as due to $^{15}N^*$ decay, and are consistent with giant-resonance excitation in the primary process.

Neutron spectra from radiative pion capture have been measured by Holland et al.,[32] Gotow et al.,[15] and Alder et al.[14] In all cases the statistical accuracy prevents very definite conclusions from being drawn. The data are consistent with giant - resonance excitation, but only Alder et al. quote a peak position; they observe a peak corresponding to 7.6 MeV excitation energy in ^{16}N when a correlated photon

with energy about 110 MeV is required.

2. Discussion of Data

In Fig. 6(c), we show our spectrum for ^{16}O. It is similar to the one from carbon, but it shows only two pronounced peaks (at 127.5 and 120.5 MeV). These peaks correspond to excitation energies in ^{16}N of 0.6 and 7.6 MeV. When the data are corrected for the energy loss in the spectrometer (0.6 MeV), we can associate the first peak with the transition to the ^{16}N ground state ($J^{\pi} = 2^-$, $I = 1$), which is separated by 10.4 MeV from the ^{16}O ground state. This state is the isospin analogue of the $J^{\pi} = 2^-$, $I = 1$ state around 13 MeV seen in inelastic electron scattering on ^{16}O.[33] We can identify the other state at 20.4 MeV; it also is seen in inelastic electron scattering. It is interesting to note that we do not see any structure corresponding to the strong peak at 18.7 MeV seen in the experiment of Ref. 33.

If we again subtract the nonresonant background by means of a pole model,[22] as in the ^{12}C case, we obtain the spectra in Figs. 6(d) and 6(e). A Q-value is used in the model corresponding to 1-MeV above the $^{15}N + n$ final state and chosen to give agreement with the data between 123 and 125 MeV. The pole-model spectrum was normalized between 60 and 90 MeV where no giant-resonance contributions are expected. Contrary to the carbon case, the normalization depends somewhat on the energy region chosen; the integral over the spectrum after subtraction can vary as much as 25% depending on whether we normalize, for example, between 60 and 80 MeV or between 80 and 100 MeV. This indicates that the pole model is not a very good description, and that the giant-resonance structure possibly extends toward lower

energies than anticipated by the model of Murphy et al.[18]

However, with no alternative description available for the non-resonant background under the peaks, we rely upon the pole model for the subtraction before comparison with the theoretical predictions for the giant-resonance region. In Fig. 6(e) these predictions, folded with the experimental resolution and efficiency, are displayed. The theoretical curve is divided by 4 and is shifted towards lower energies by 1 MeV to match the position of the 2^- state and that of the peak and observed in the data. In addition to this dipole state, the theoretical spectrum contains transitions to quadrupole states: $J^\pi = 1^+$ at 111 MeV, $J^\pi = 2^+$ at 112 MeV, and $J^\pi = 3^+$ at 119.5 MeV. It is the contribution from these which causes the poor agreement with the data, which we will now show.

The total radiative branching ratio was measured to be $(2.24 \pm 0.48)\%$. It was determined by calculating from range curves with thinner targets the fraction of pions stopping in the region considered in the cut spectrum. We obtain the same result from a smaller sample of data taken with a water target. The partial branching ratios are $(1.84 \pm 0.38)\%$ for the pole-term contribution and $(0.15 \pm 0.03)\%$ for the ground-state transition, leaving $(0.25 \pm 0.06)\%$ for the giant-resonance absorption. The theoretical predictions for the rates to giant-resonant transitions are $\Lambda_{1s}^{rad} = 5.1 \times 10^{17}\ sec^{-1}$ and $\Lambda_{2p}^{rad} = 1.1 \times 10^{14}\ sec^{-1}$. Using these quantities and the total nuclear absorption rates (appropriately weighted, as discussed earlier), we obtain for the fraction of pions which undergo radiative capture to giant-resonance states 0.38% for the 1s and 1.40% for the 2p state, or total 1.78%. This value is to be compared with the 0.32% observed. This discrepancy is

striking, even considering the possible large errors in the subtraction of the nonresonant background. If we fit all the events between 112 and 122 MeV to one Breit-Wigner resonance (see Table III), we obtain a partial experimental branching ratio of 0.22% (in agreement with the value of Alder et al.[14] of 0.2%), while the theoretical value obtained by Murphy et al.[18] for the branching ratio to the 2^- is 0.43%. In this calculation the rescattering terms were neglected. If one includes these, a reduction of the partial capture rate of as much as 40% can be expected,[7] which would bring theory and experiment into agreement. However, the rescattering has been considered for 1s capture only. In the same calculation[7], the ratio of the 1s capture rates to the ground state and to the 2^- state is approximately 2 to 1, fairly close to that observed in our experiment for the combination of 2p and 1s capture.

We conclude that our data indicate that quadrupole states are not excited in ^{16}O, when absolute rates are considered. From the structure of the spectrum alone, we cannot fully exclude their existence. (See results of a two-Breit-Wigner fit to the giant-resonance region of the data, summarized in Table III and Fig. 6d.)

We conform our findings from ^4He and ^{12}C, in that the simple form of the π-capture matrix element combined with collective dipole excitations gives a good picture of the radiative pion capture process. For the ground-state transition, no predictions exist; this is unfortunate since it would be another prime candidate for the determination of the axial vector form factors, if the 2p capture could be handled properly.

D. Magnesium and Calcium

Muon capture in ^{40}Ca has been studied by Igo-Kemenes et al.[34] in a similar manner to the ^{16}O studies of Kaplan et al.,[13] that is by measuring the low-energy gamma-ray spectrum of the products of the capture process. As with ^{16}O, these are quite similar to the spectra observed after photoexcitation and are consistent with some giant-resonance excitation. Evseyev et al.[11] have measured the neutron spectrum following muon capture in ^{40}Ca, but no strong conclusions regarding resonance excitation can be drawn.

Our experimental spectra for magnesium and calcium are presented in Figs. 7 and 8, respectively. No dominant structure is observed in either. The pole-model predictions are also shown; but they do not seem to represent the data well, possibly indicating that with increasing mass number the question of the initial state of the nucleon inside the nucleus, which is neglected in the peripheral model, becomes more important. No detailed theoretical predictions exist for either element, although for ^{40}Ca it was shown[35] that the distribution of spin-isospin strength among levels of given J^{π} is rather badly fragmented. For 2p absorption and the 1^- states in ^{40}K, the following transition strengths are obtained (in percent) for levels at the indicated energies (relative to the ^{40}Ca ground state): 14.9 MeV (17%), 12.8 MeV (27%), 8.7 MeV (7%), 7.3 MeV (5%), 6.1 MeV (13%), 4.8 MeV (5%), 4.0 MeV (9%), and 2.5 MeV (17%). The levels should be observed at γ energies of 124.0, 126.1, 126.1, 130.2, 131.6, 132.8, 134.1, 134.9, and 136.4 MeV. None of these levels can be identified with the minor structures seen at 115, 119, and 128 MeV. The states above 130 MeV are possibly excited since there are events above the

$^{39}K + n$ threshold; but they are too close to be resolved with our apparatus. The total fraction of pions undergoing radiative capture is $(2.15 \pm 0.20)\%$ for magnesium and $(1.94 \pm 0.18\%$ for calcium.

ACKNOWLEDGMENTS

We would like to acknowledge the continued cooperation of James Vale and members of the 184-inch cyclotron crew. Also, Dennis Soon, Patrick Craig, Roger Bell, and many others have contributed their skills in scanning and measuring the film.

APPENDIX: PION CAPTURE IN HYDROGENOUS COMPOUNDS

The relative probability for capturing pions in bound hydrogen in hydrogenous compounds has already been measured in several earlier experiments. All experiment used the same technique. Since the charge-exchange reaction for pions at rest is energetically prohibited in most nuclei, one can from the known yield for the charge-exchange reaction on hydrogen directly determine the desired relative capture probability (f) by measuring the π^0 yield from (for example) a CH_2 target. This technique has one difficulty, arising from the unknown contributions from charge-exchange reactions occurring in-flight. The experimental values have therefore fluctuated somewhat over the various experiments. In light of this fact, and the fact that a theory for the capture probability[36] has recently become available which explains the deviations from the older Fermi-Teller Z-law ($f \sim 1/Z$),[37] we have remeasured f with a different method. With our energy resolution, the 129.4-MeV hydrogen line appears as a sharp peak in the photon spectrum from radiative pion capture from any H_nZ_m target (see Fig. 9). With the known spectra and the yields for the individual compounds, the H_nZ_m spectrum can be fitted with a linear combination of individual spectra. We have tried our method on CH_2 and H_2O targets, and have obtained results in excellent agreement with the average values from all previous experiments (Table IV). Our accuracy was limited due to statistics since this investigation was not the primary goal of our experiment. The agreement demonstrates the usefulness of our method, especially for higher Z where the in-flight corrections become severe for the charge-exchange method (~ 25% for Ca).[38] In Fig. 10 we have compared our results and the previous

measurements with the theoretical predictions of the model of Ponomarev.[36] This model assumes that the pion in the slowing-down process is captured into orbits common to the whole molecule. From this stage, the relative probabilities for the formation of a proton-mesic or a nucleus-mesic atom can be calculated. The relative probability for capture on hydrogen (f) follows the law $(m/n + 1/Z) \times f = a_L/Z^3$, with a_L being an empirical constant; and is found to be 1.28 for L = 2.[38] The agreement between this theory and the experimental values is satisfactory.

FOOTNOTES AND REFERENCES

*Work done under the auspices of the U. S. Atomic Energy Commission.

†Present address: Rutherford Laboratory, Chilton, Berkshire, England.

††Present address: CERN, 1211 Geneva 23, Switzerland.

‡Present address: Physik-Institut der Universitat Zürich, 8001 Zürich, Switzerland.

1. J. A. Bistirlich et al., Phys. Rev. Letters 25, 950 (1970).
2. J. A. Bistirlich et al., Phys. Rev. Letters 25, 689 (1970).
3. J. Delorme and T. E. O. Ericson, Phys. Letters 21, 98 (1966); H. Pietschmann et al., Phys. Rev. Letters 19, 1259 (1967); Griffiths and C. W. Kim, Nucl. Phys. B4, 309 (1968).
4. J. Delorme, Nucl. Phys. B13, 573 (1970).
5. M. Ericson and A. Figureau, Nucl. Phys. B3, 609 (1967).
6. A. Raiche and K. Werntz, Preprint, Catholic University of America (1971).
7. R. Guy and J. M. Eisenberg, Nucl. Phys. B11, 601 (1969).
8. J. P. Deutsch et al., Phys. Letters 26B, 315 (1968).
9. D. K. Anderson and J. M. Eisenberg, Phys. Letters 22, 164 (1966).
10. L. L. Foldy and J. D. Walecka, Nuovo Cimento 34, 1026 (1964); J. Barlow et al., Phys. Letters 9, 84 (1964); V. V. Balashov et al., Phys. Letters 9, 168 (1964).
11. V. Evseyev et al., in High Energy Physics and Nuclear Structure, S. Devons, Ed. (Plenum Press, New York, 1920), p. 157.

12. M. E. Plett and S. E. Sobotka, Phys. Rev. 36, 1003 (1971).

13. S. N. Kaplan et al., Phys. Rev. Letters 22, 795 (1969).

14. J. C. Alder et al., Nuovo Cimento Letters 4, 256 (1970).

15. K. Gotow et al., in High Energy Physics and Nuclear Structure, S. Devons, Ed. (Plenum Press, New York, 1970), p. 374.

16. H. Davies et al., Nucl. Phys. 78, 673 (1966).

17. F. J. Kelly and H. Überall, Nucl. Phys. A118, 302 (1968).

18. J. D. Murphy et al., Phys. Rev. Letters 19, 714 (1967).

19. G. Schnurmacher et al., Nucl. Instr. Methods 60, 89 (1968).

20. V. T. Cocconi et al., Nuovo Cimento 22, 494 (1961).

21. J. A. Bistirlich et al., in High Energy Physics and Nuclear Structure, S. Devons, Ed. (Plenum Press, New York, 1970). p. 497.

22. L. G. Dakhno and Yu. D. Prokoshkin, Sov. J. Nucl. Phys. 7, 129 (1968).

23. For a discussion of this indirect method of determining the width of the 2p-level see G. Backenstoss, Ann. Rev. Nucl. Sci. 20, (1970), p. 467. We have neglected here the small contribution for auger transitions.

24. H. Hilscher et al., Nucl. Phys. A158, 584 (1970).

25. W. Sapp, Thesis, College of William and Mary (1970), unpublished.

26. W. E. Meyerhof and T. A. Tombrello, Nucl. Phys. A119, 1 (1968).

27. S. Berezin et al., Phys. Letters 30B, 27 (1969).

28. F. H. Lewis and J. D. Walecka, Phys. Rev. 133B, 849 (1964).

29. M. Kamimura et al., Nucl. Phys. A95, 125 (1967).

30. E. J. Maier et al., Phys. Rev. 133B, 66 3 (1964).

31. W. H. Maguire and C. Werntz, Preprint, Catholic University of America (1971).

32. M. M. Holland et al., in High Energy Physics and Nuclear Structure, S. Devons, Ed. (Plenum Press, New York, 1970), p. 538.

33. I. Sick et al., Phys. Rev. Letters 23, 1117 (1969).

34. P. Igo-Kemenes et al., Phys. Letters 34B, 286 (1971)

35. R. Guy and J. M. Eisenberg, Phys. Letters 33B 137 (1970).

36. L. T. Ponomarev, Sov. J. Nucl. Phys. 2, 160 (1966).

37. E. Fermi and E. Teller, Phys. Rev. 72, 399 (1947).

38. Z. V. Krumstein et al., Sov. Phys.-JETP 27, 906 (1963).

39. The spectra with efficiency divided out are shown for illustrative purposes only. In order to compare theoretical predictions with data, they have to be folded with the experimental resolution first (low energy tail and shift in energy) and then multiplied with the experimental efficiency. If just the experimental efficiency is divided out, errors up to 5% in absolute magnitude can be introduced.

Table I. Contributions to the experimental capture rates.

Element	Target mass (g/cm^2)	Number of photons in the spectrum						Number of pions stopped			Radiative pion capture rate (%)
		N_1 [a]	N_2 [b]	N_3 [c]	N_4 [d]	N_5 [e]	N_0 [f] ($\times 10^8$)	P_1 [g] ($\times 10^{10}$)	P_2 [h] ($\times 10^{10}$)	P_0 [i] ($\times 10^{10}$)	
^4He	5.7	6955 ± 84		4238 ± 98	5051 ±117	5890 ±139	2.71 ±0.15	3.62	2.00 ±0.30	1.81 ±0.28	1.50 ± 0.29
^{12}C	5.6	6590 ± 81		5432 ±341	7167 ±450	7590 ±475	3.49 ±0.28	2.32	1.92 ±0.10	1.82 ±0.10	1.92 ± 0.19
^{16}O	39.1 [j] (12.8)	9614 ± 98	4303 ± 66	3122 ± 69	4042 ±262	5940 ±386	2.73 ±0.22	2.52 [j]	1.38 ±0.26	1.22 ±0.24	2.24 ± 0.48
^{24}Mg	4.1	5065 ± 71		4313 ±173	5670 ±232	6240 ±256	2.87 ±0.19	1.79	1.43 ±0.08	1.38 ±0.08	2.08 ± 0.21
^{40}Ca	7.3	7070 ± 84		6208 ± 87	7730 ±109	9450 ±133	4.35 ±0.22	2.79	2.50 ±0.14	2.39 ±0.15	1.82 ± 0.15
$^{12}CH_2$ (^{12}C)	5.0	1785 ± 59		1297 ±144	1711 ±190	1798 ±200	0.83 ±0.10	0.57	0.516 ±0.024	0.503 ±0.025	1.64 ± 0.21
$^{16}OH_2$ (^{16}O)	12.7	1115 ± 33		710 ± 87	916 ±113	1050 ±130	0.482 ±0.064	0.256	0.248 ±0.016	0.248 ±0.019	2.20 ± 0.33
H_2 ($n\gamma$)	3.2	948 [k] ± 31			948 ± 31	1100 ± 36	0.501 ±0.030	0.0184	0.0121 ±0.0006	0.0121 ±0.0006	41.4 ± 3.2 [k]
H_2 ($n\pi^0$)	3.2	890 [l] ± 30			1361 ±158	1581 ±184	0.728 ±0.092				60.0 ± 8.2 [l]
Panofsky Ratio						1.44 ±0.17					

a. Raw number of events.
b. Number of events after cut in the distribution of origin of the photons in the target.
c. Number of events after subtraction of the background due to pions captured in flight and to background from the target container.
d. Number of events corrected for events with energies below 50 MeV and for the energy-dependent efficiency, normalized to $\eta_\gamma(E_\gamma = 130\ \text{MeV}) = 1$.
e. Number of events corrected for loss of photons due to conversion in the target and in surrounding material other than the converter.
f. Number of photons into full solid angle.
g. Raw number of beam particles stopped in the target.
h. Number of pions interacting in the target after correction for contaminations, stops in material other than the target itself, and electronic and geometric inefficiencies in the detector setup.
i. Number of pions stopping in the target after correction for pions interacting in flight.
j. This number is for the full oxygen dewar, not only for the region considered for the cut spectrum.
k. Radiative capture only: $\pi^- p \rightarrow n\gamma$.
l. Mesonic capture only: $\pi^- p \rightarrow n\pi^0$.

0 0 0 0 3 7 0 1 0 2 9

Table II. Parameters, taken from pionic X-ray data, used in deriving the capture probabilities from Bohr orbtis. Several values are available for the primary data; we have taken an average (shown underlined) excluding those value shown in parenthesis.

Element	$\Gamma_{2p \to 1s}$ Measured (keV)	Λ^{tot}_{1s} (sec^{-1})	$\Lambda^{e.m.}_{2p \to 1s}$ (sec^{-1})	Yield$_{(2p \to 1s)}$	Population (2p)	$\omega_{1s} = \frac{Y_{(2p \to 1s)}}{P_{(2p)}}$	Λ^{tot}_{2p} (sec^{-1})
^{12}C				0.076±0.009[a]			
	2.96±0.25[b]			0.075±0.02[b]			
	2.60±0.50[c]			0.082±0.006[c]			
	3.25±0.15[d]			[0.035±0.010[e]]	[0.067±0.04[e]]		
	3.12±0.12 (average)	$0.474 \pm 0.018 \times 10^{19}$	2.14×10^{14}	0.080±0.005 (average of first three)	0.062±0.06[b]	0.129±0.015	$1.43 \pm 0.19 \times 10^{15}$
^{16}O	7.56±0.60[b] (9.0 ±2.0[c])	$1.149 \pm 0.076 \times 10^{19}$	6.70×10^{14}	0.049±0.007[b] (0.020±0.005[e])	0.57 ±0.06[b] (0.57 ±0.04[e])	0.086±0.015	$7.12 \pm 1.2 \times 10^{15}$

a. M. Camac et al., Phys. Rev. 99, 897 (1955).
b. Backenstoss, Ann. Rev. Nucl. Sci. 20, 467 (1970).
c. A. C. Kunselman, Thesis, University of California, Berkeley, UCRL-18654 (1969), unpublished.
d. R. J. Harris et al., Phys. Rev. Letters 20, 505 (1968).
e. W. Sapp, Thesis, College of William and Mary (1970), unpublished.

Table III. Experimental and theoretical parameters of radiative capture spectra. Errors in experimental quantities are statistical only. The absolute uncertainty in the energy scale is 0.5 MeV. The absolute rates quoted contain all errors summarized in Table I.

Element	Experimental parameters of peaks and continuum			Energy levels derived from expermental E		Theoretical predictions			
	E_γ (MeV)	Γ_γ (MeV)	$\Lambda^{rad}/\Lambda^{tot}$ (%)	$E(I_3=-1)$ (MeV)	$E(I_3=0)^k$ (MeV)	ω^j (MeV)	J^π	$E(I_3=0)^k$ (MeV)	$\Lambda^{rad}/\Lambda^{tot}$ (%)
^{4}He	113.2			3.4[b]		24.6	2^-		
	111.0			(5.1[b])		26.8	1^-		
	108.5			(7.4[b])		28.4	1^-		
			1.50 ±0.009 (Total)						2.1±0.7[c] (Total)
^{12}C	124.65±0.05	0.31±0.08	0.091±0.009	0.35	15.45	13.4	1^+	15.1	0.087±0.030[n]
	(124.45±0.20)[a]	(0.95±0.65)[a]	(0.135±0.035[a]						
	120.25±0.05	0.45±0.12	0.185±0.019	4.75	19.85	19.1	2^-[e]	20.8	0.153±0.022[e]
	116.90±0.11	1.09±0.13	0.159±0.016	8.10	23.20	21.1	1^-[e]	23.3	0.038±0.002[e]
						23.3.	1^-[e]	25.0	0.139±0.007[e] 0.224
						22.3	2^-	24.0	0.047±0.008[e] ±0.017
	Particle-unstable states		0.344±0.034			Particle-unstable states			0.500±0.045
	Pole contribution[h]		1.491±0.151						
		Total	1.92 ±0.199 (1.60 ±0.10)[d]			Total			2.3[f] 1.09[g]
^{16}O	128.10±0.05[l]	0.11±0.02	0.15 ±0.03	0	13.0	10.4	2^-[i]	13.0	
	120.40±0.05[l]	1.44±0.11[l]	0.22 ±0.05[l]	7.70	20.7	17.5	2^-[i]	20.1	0.43 ±0.06[i]
	120.70±0.05[m]	0.13±0.07[m]	0.11 ±0.02[m]	8.00	21.0	17.5	2^-[i]	20.1	0.43 ±0.06[i]
	117.30±0.24[m]	2.94±0.71[m]	0.13 ±0.04[m]	10.40	23.4	22.0	1^-[i]	24.6	0.28 ±0.04
						22.5	0^-	25.1	
	Particle-unstable states		0.25 ±0.06			Particle-unstable states			1.78 ±0.27[i]
	Pole contribution		1.84 ±0.39			Dipole states only			0.71 ±0.09[i]
		Total	2.24 ±0.48						

a. These values are derived from the CH_2 spectrum. The energies therefore have an uncertainty of only 0.1 MeV. The partial capture rate is based on a relative pion capture probability of (1.19 ± 0.06)%.
b. Energy levels in ^{4}H are relative to the ^{3}H + n threshold. Only the position of the 2^- was determined from the experiment; the positions of the two 1^- states were left fixed their theoretical values.
c. A. Raiche and K. Werntz, Ref. 6.
d. H. Davies et al., Ref. 16.
e. Energy levels and brancing ratios are those derived by F. D. Kelly and H. Überall, from the model of F. H. Lewis, J. D. Walecka, Ref. 8.
f. J. Delorme, T. E. O. Ericson, Ref. 3.
g. D. K. Andersen, J. M. Eisenberg, Ref. 9.
h. The pole contributions have been corrected for events below E_γ = 50 MeV.
i. J. D. Murphy et al., Ref. 18.
j. Excitation energy in ^{4}H, ^{12}B, or ^{16}N measured from the ^{4}He, ^{12}C, or ^{16}O ground state, respectively.
k. Excitation energy in the parent nucleus for the I_3 = 0 analogous state (for comparison with inelastic electron scattering data).
l. Results of two Breit-Wigner resonances fit.
m. Results of three Breit-Wigner resonances fit.
n. W. Maguire and C. Werntz, Ref. 31.

Table IV. Relative pion capture probabilities in hydrogenous compounds.

LiH	CH	CH_2	H_2O	Reference
		0.77 ± 0.13[a]		1. M. V. Terentév, Sov. Phys., JETP 17, 890 (1963).
3.3 ± 0.4	0.41 ± 0.05	1.06 ± 0.10	0.26 ± 0.04	2. A. F. Dunaitsev et al., Nuovo Cimento 34, 527 (1964).
3.9 ± 0.3	0.54 ± 0.05	1.39 ± 0.11		3. P. Depommier et al., Phys. Letters 5, 61 (1963).
4.0 ± 0.4	0.55 ± 0.07	1.79 ± 0.19		4. D. Bartlett et al., Phys. Rev. 136B, 1453 (1964).
3.5 ± 0.4	0.51 ± 0.06	1.32 ± 0.15	0.35 ± 0.06	5. Z. V. Krumstein et al., Sov. Phys. JETP 27, 906 (1968).
3.72 ± 0.18	0.487 ± 0.028	1.19 ± 0.06	0.289 ± 0.033	Weighted average
		1.06 ± 0.15	0.192 ± 0.110	This experiment

a. Corrected value quoted by A. F. Dunaitsev et al., Experiment 2 above.

FIGURE CAPTIONS

Fig. 1. Experimental layout. The mirror system for photography of spark chambers and the details of the magnet coils are omitted for clarity. The trigger for an event was $\pi_1 \times \pi_2 \times \pi_3 \times \bar{\pi}_S \times \bar{\pi}_C \times A_i \times B_i \times A_k \times B_k$; $i \neq k$, $k \pm 1$.

Fig. 2. Photon energy spectrum for π^- capture in hydrogen (1-MeV bins). The insert shows the events from radiative capture in 0.2-MeV bins, used as the experimental resolution function.

Fig. 3. Efficiency of the pair-spectrometer as a function of the photon energy.

Fig. 4. Energy spectrum of photons from radiative pion capture in ^{4}He. (a) Spectrum with the efficiency divided out.[39] (b) Measured spectrum corrected for target-out and in-flight-capture contributions. The solid line represents the theoretical curve of K. Werntz, as reported in Ref. 1, for 1s capture only. The dashed curve is from A. Raiche and K. Werntz, Ref. 6, where only their calculation for 1s-capture was used, since it accounts for 90% of the total capture rate; the normalization factor is 0.8, well within the 30% error of the absolute rate.

Fig. 5. Pion capture in ^{12}C. (a) Spectrum with the efficiency divided out. (b) Measured spectrum; solid curve is the pole-model contribution. (c) Resonant contributions; i.e., after subtraction of the pole-model part. Solid curve is the three-Breit-Wigner resonance fit to the data. Dashed curve is the prediction by F. J. Kelly and H. Überall, Ref. 17, folded with experimental

resolution and efficiency, and normalized for the number of pions stopped in the target. The curve is shifted towards lower energies by 2 MeV.

Fig. 6. Energy spectrum of photons from radiative pion capture in ^{16}O.

(a) Raw spectrum.

(b, c) Spectrum after cut in the distribution for the origin of the photons within the target and after subtraction of the background from pion capture occuring in flight.

(b) With the energy-dependent efficiency divided out.[39]

(c) Solid curve: pole-model contribution.

(d, e) Resonant contributions, i.e., the spectrum after subtraction of the pole-model contribution.

(d) Two and three Breit-Wigner resonance fits to the data between 110 and 130 MeV.

(e) Theoretical curves from Murphy et al.: 1s and 2p capture added with proper weights and folded with experimental resolution and efficiency. Curves are shifted by 1.5 MeV. Solid line: all states (theory divided by 4); dashed line: $J = 2^-$, $I = 1$ state only (divided by 2).

Fig. 7. Energy spectrum of photons from radiative pion capture in magnesium. (a) Spectrum with efficiency divided out.[39] (b) Measured spectrum with in-flight background subtracted; solid line: pole-model predictions.

Fig. 8. Energy spectrum of photons from radiative pion capture in calcium. (a) Spectrum with efficiency divided out.[39] (b) Measured spectrum with in-flight background subtracted; solid line: pole-model predictions.

Fig. 9. Photon energy spectrum from π^- capture in CH_2.

Fig. 10. Relative probability for the capture of pions on protons in hydrogenous compounds. Plotted is the reduced probability $P = (m/n + 1/Z) \times f$, where f is the measured probability, m and n the number of atoms in the compound $H_n Z_m$. The solid line is the theoretical prediction from the "meso-molecule" assumption, Ref. 36.

■ This experiment.

● Z. V. Krumstein, Ref. 38.

O World average, taken from Table IV.

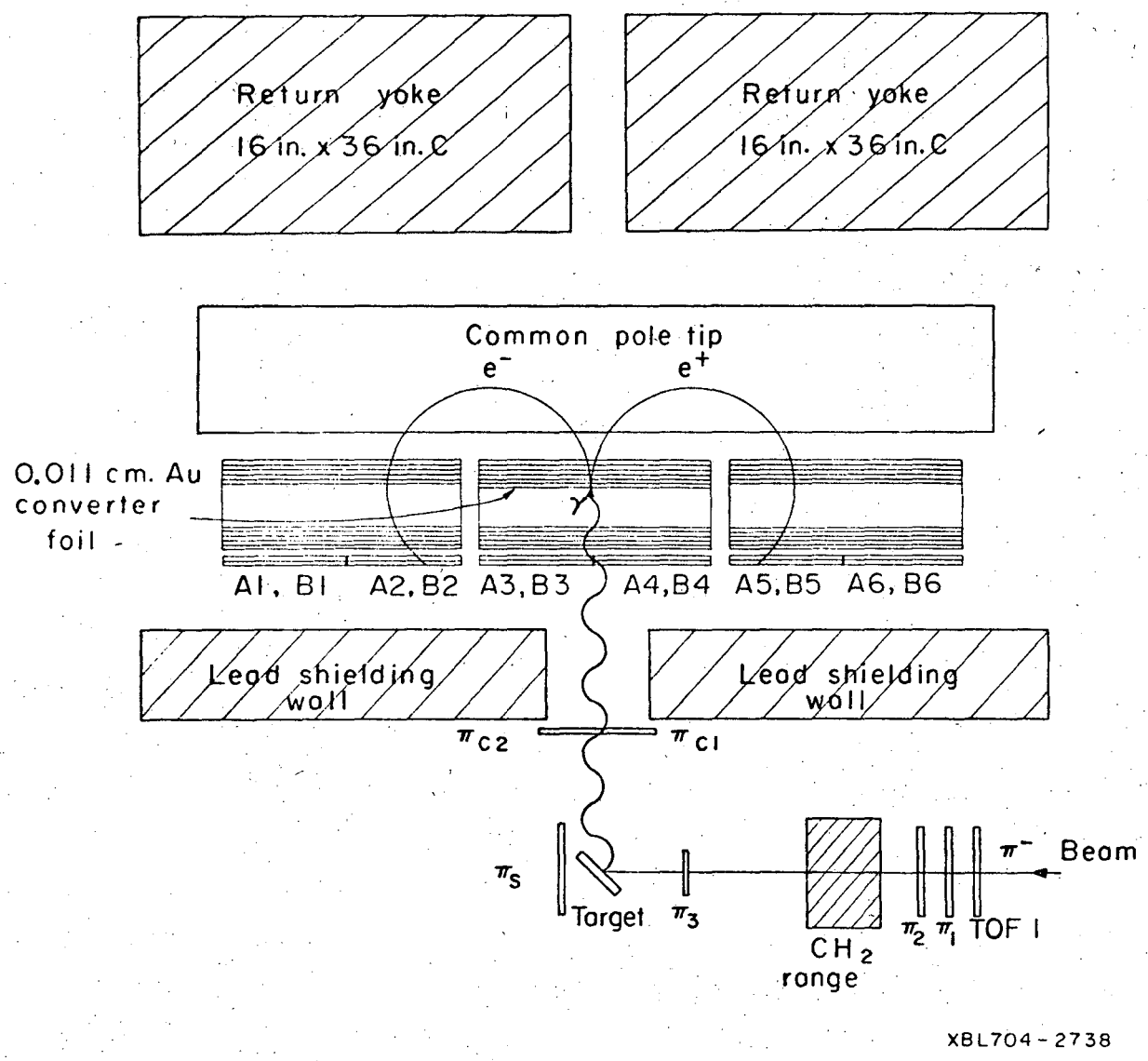
Return yoke
16 in. x 36 in. C
Return yoke
16 in. x 36 in. C
Common pole tip
e⁻
e⁺
0.011 cm. Au
converter
foil
γ
A1, B1
A2, B2
A3, B3
A4, B4
A5, B5
A6, B6
Lead shielding
wall
Lead shielding
wall
πc2
πc1
πs
Target
π3
CH2
range
π2
π1
TOF I
π⁻
Beam
XBL704-2738

Fig. 1

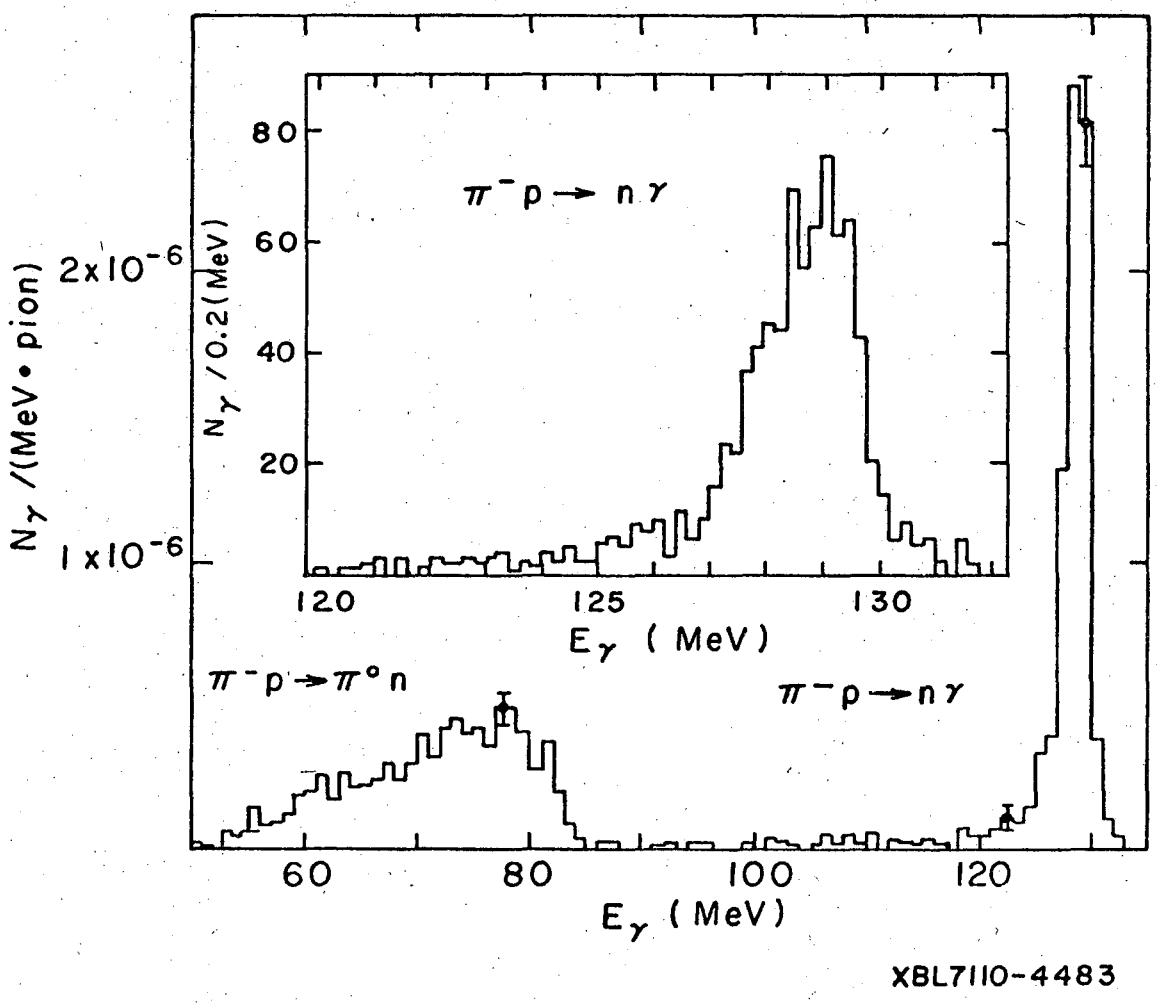
N_γ /(MeV • pion)
2×10^{-6}
1×10^{-6}
$\pi^- p \rightarrow \pi^0 n$
$\pi^- p \rightarrow n\gamma$
60
80
100
120
E_γ (MeV)
N_γ /0.2(MeV)
80
60
40
20
$\pi^- p \rightarrow n\gamma$
120
125
130
E_γ (MeV)
XBL7110-4483

Fig. 2

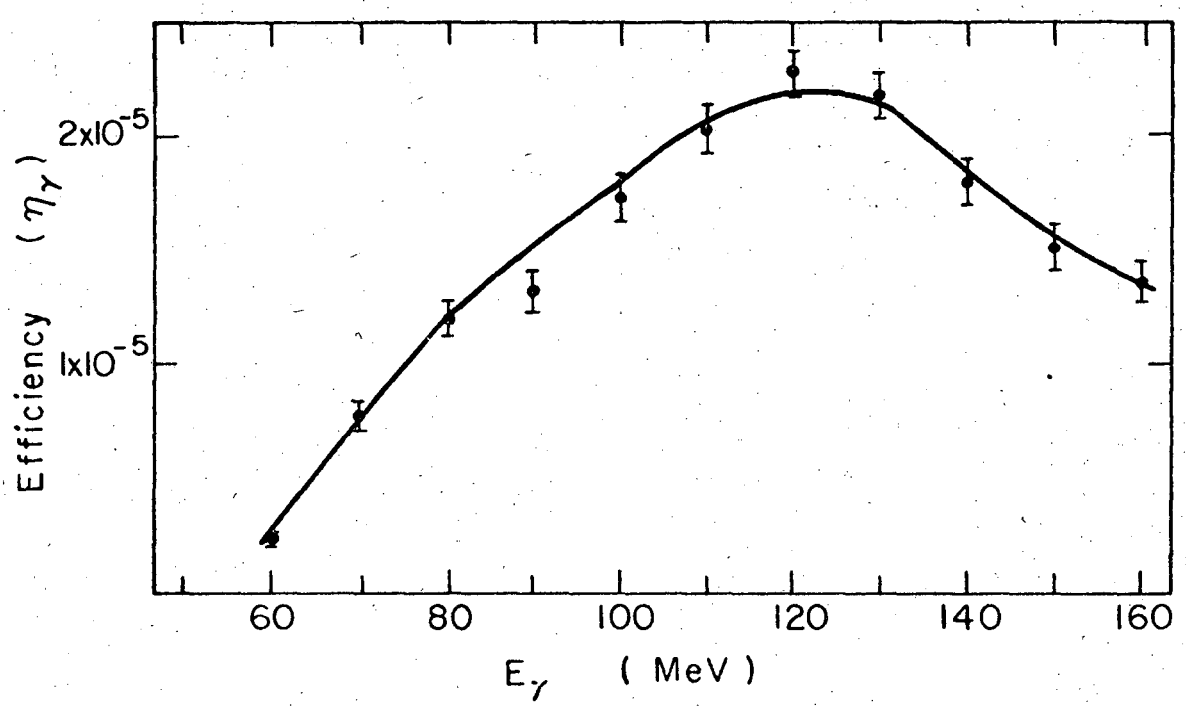

XBL7110-4484

Fig. 3

0 0 0 0 3 7 0 1 0 3 3

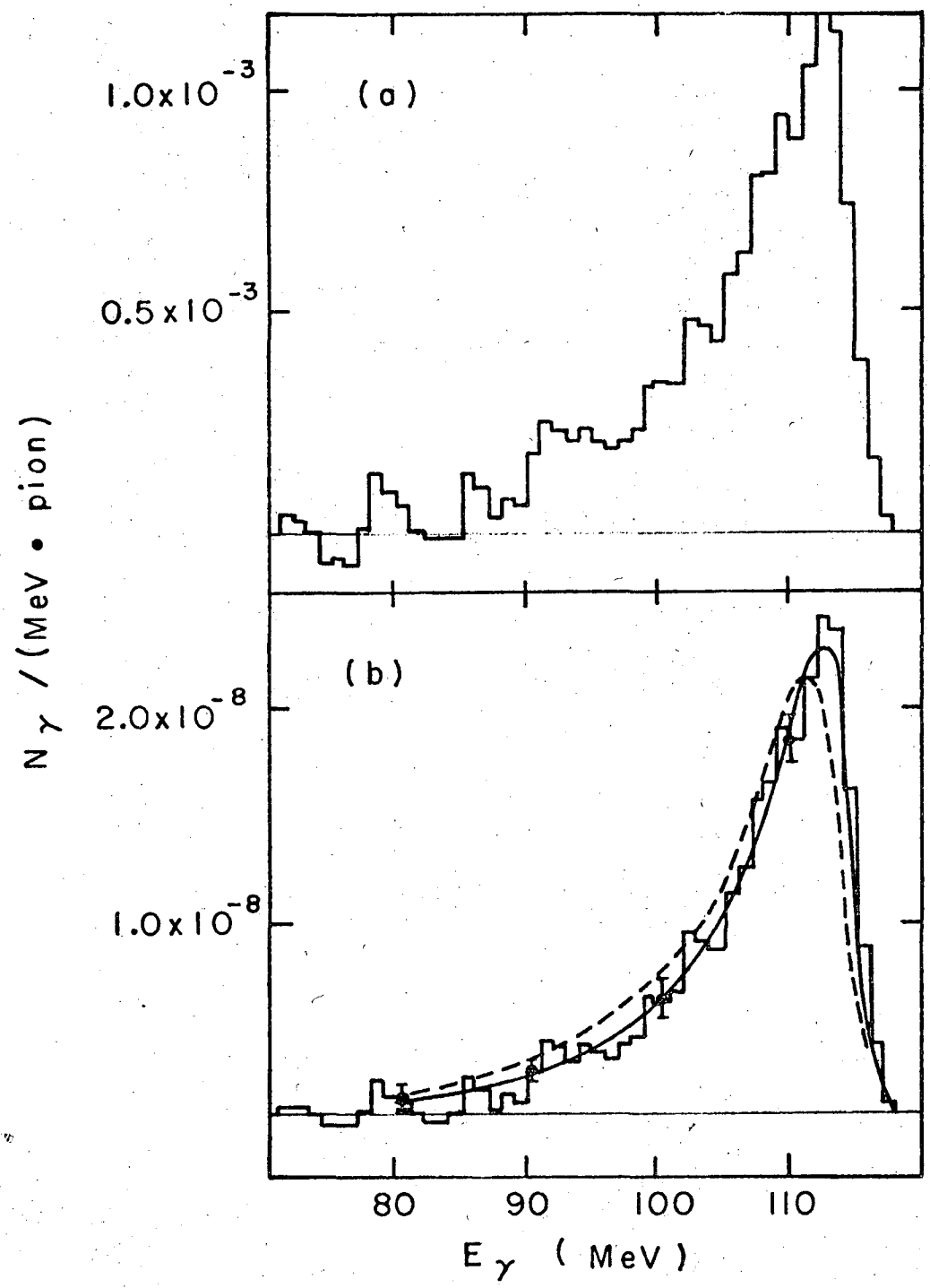

XBL 7110-4485

Fig. 4

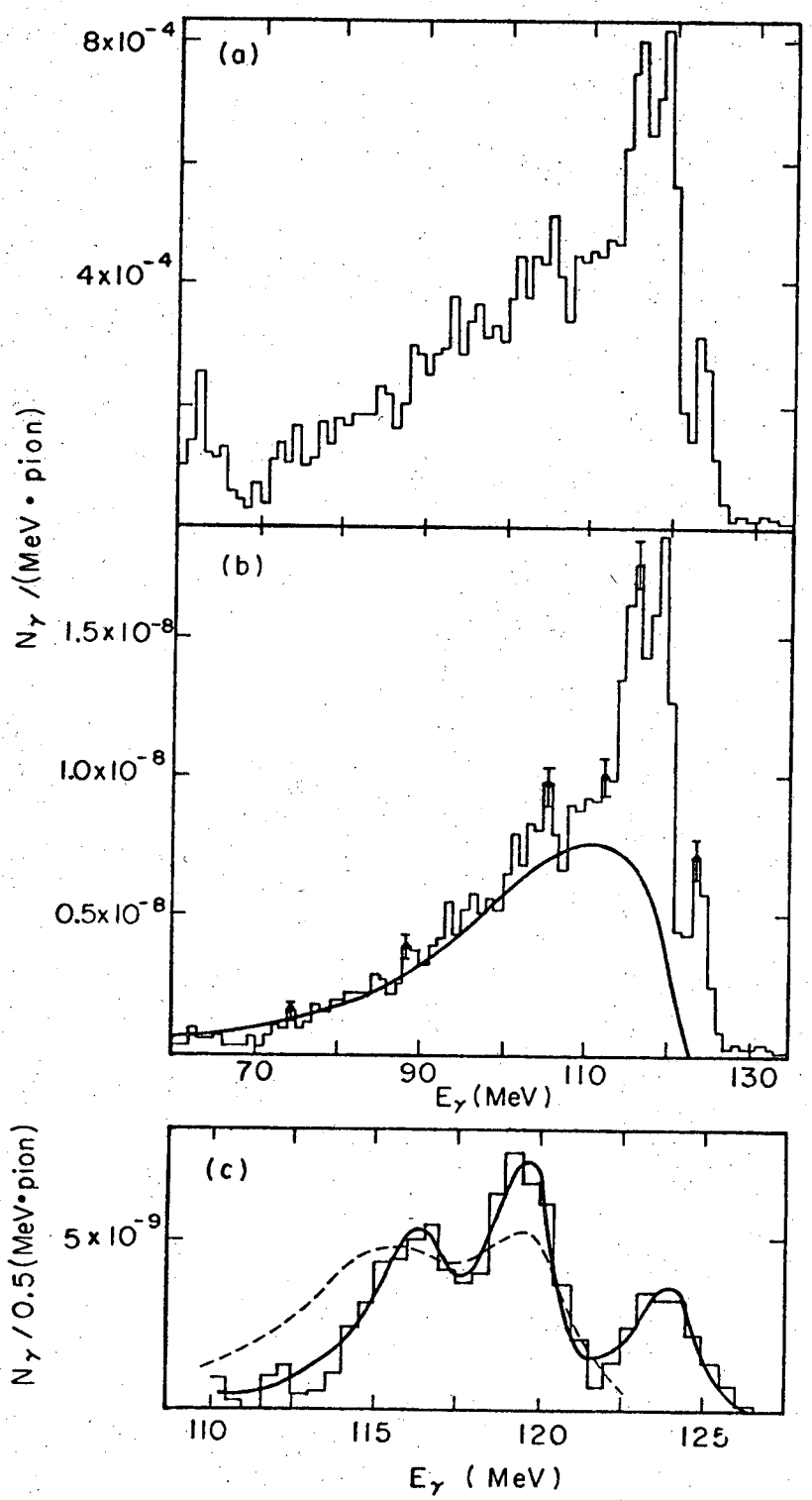

XBL7110-4486

Fig. 5

0 0 0 0 3 7 0 1 8 3 4

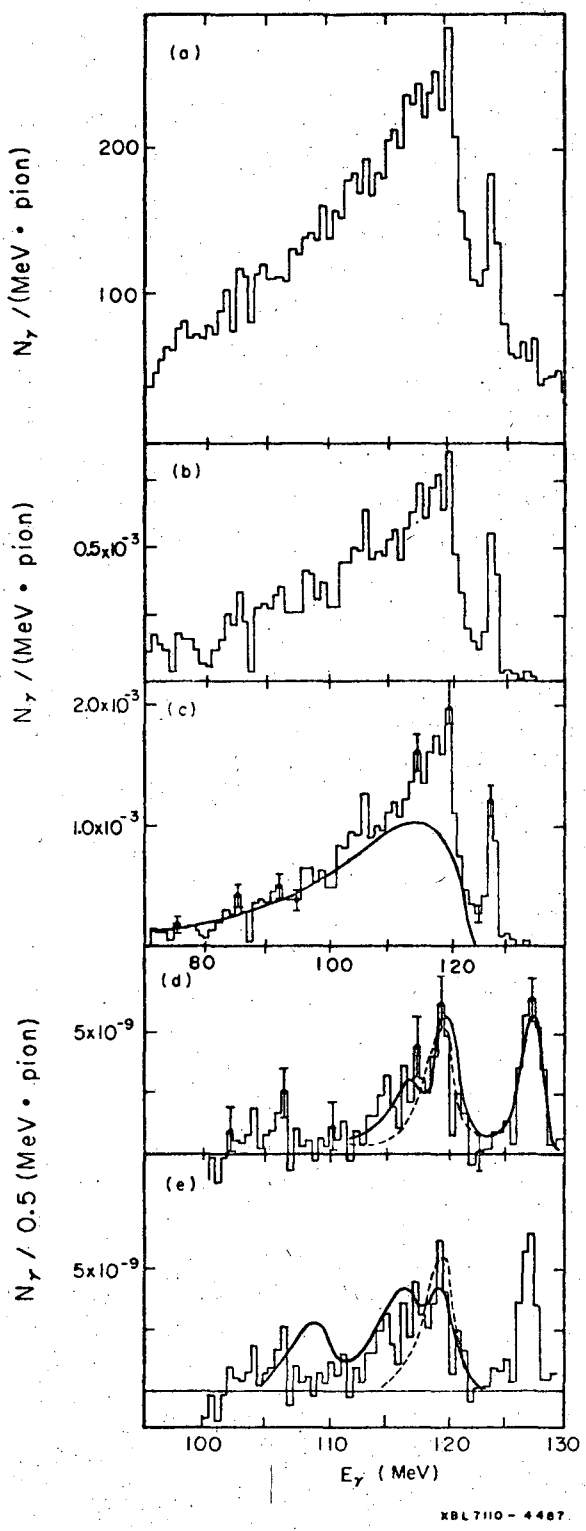

Fig. 6

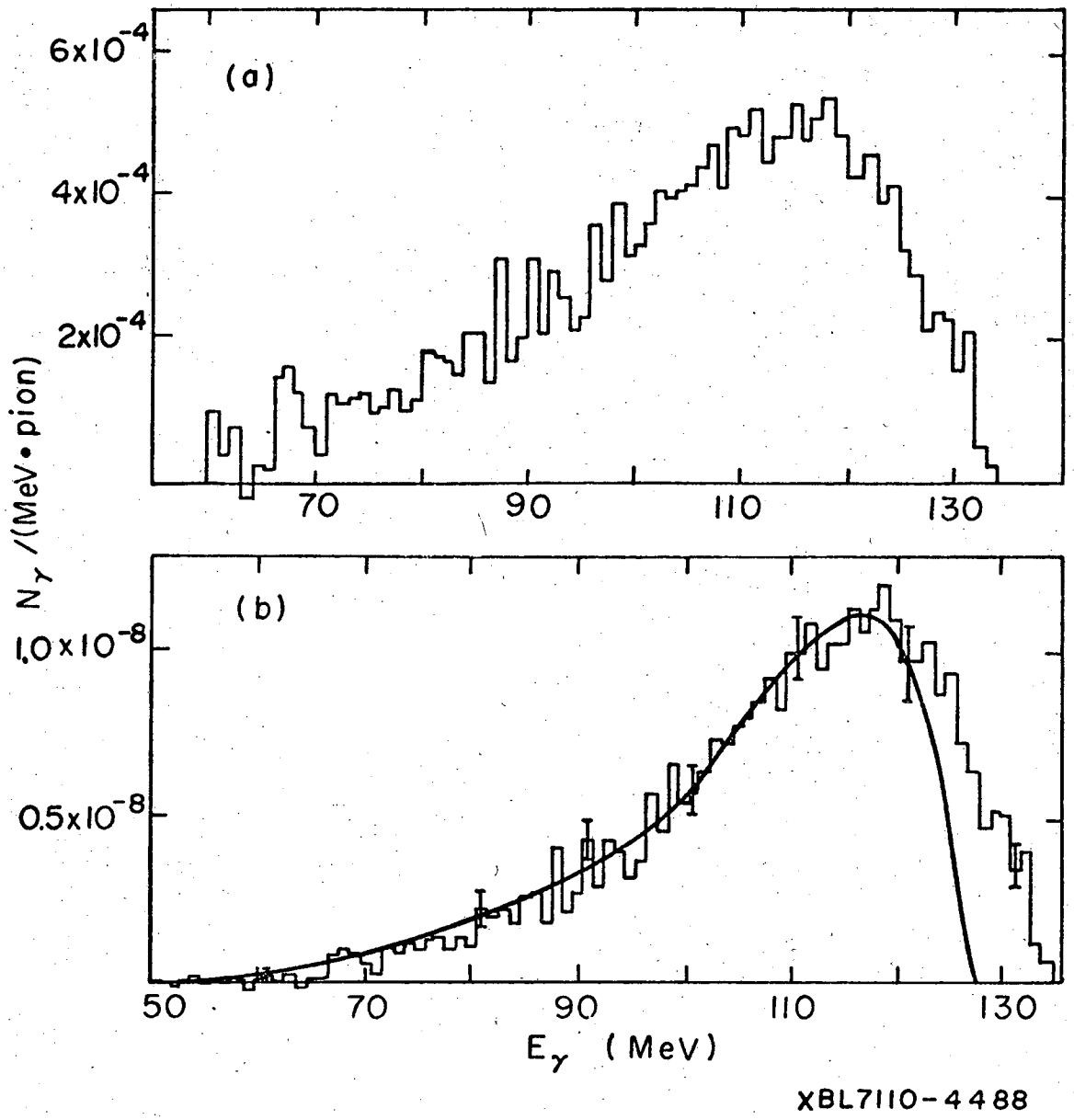
6x10^-4
4x10^-4
2x10^-4
(a)
70
90
110
130
N_γ /(MeV • pion)
(b)
1.0x10^-8
0.5x10^-8
50
70
90
110
130
E_γ (MeV)
XBL7110-4488

Fig. 7

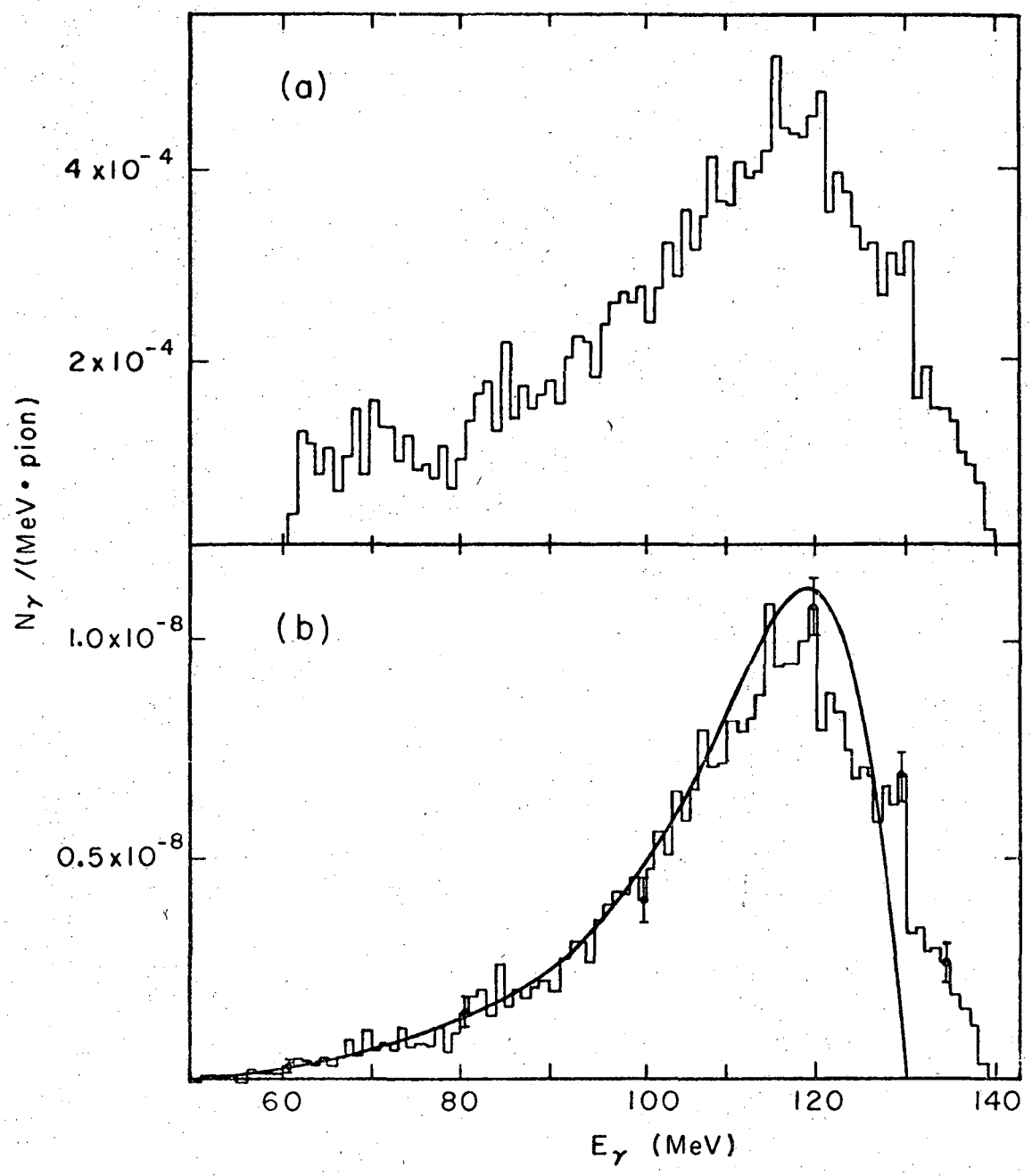

XBL7110-4489

Fig. 8

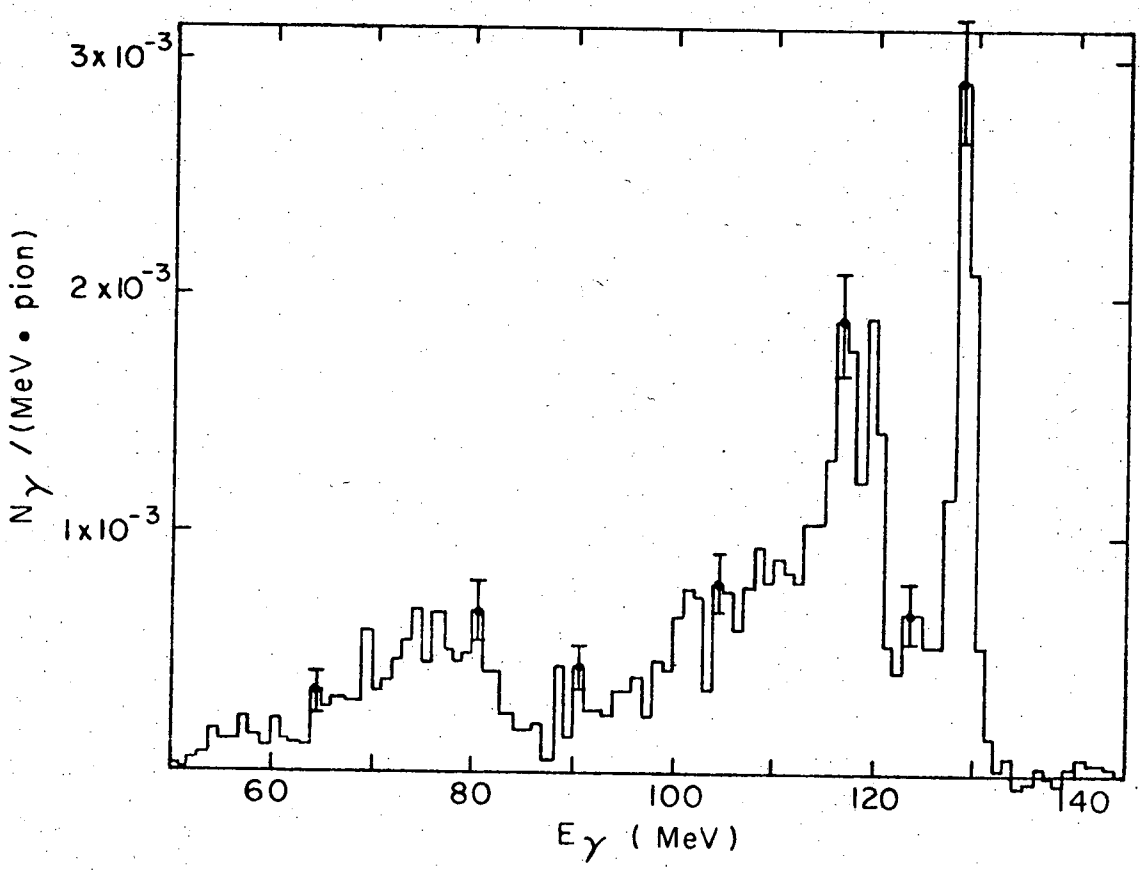

XBL 7110-4490

Fig. 9

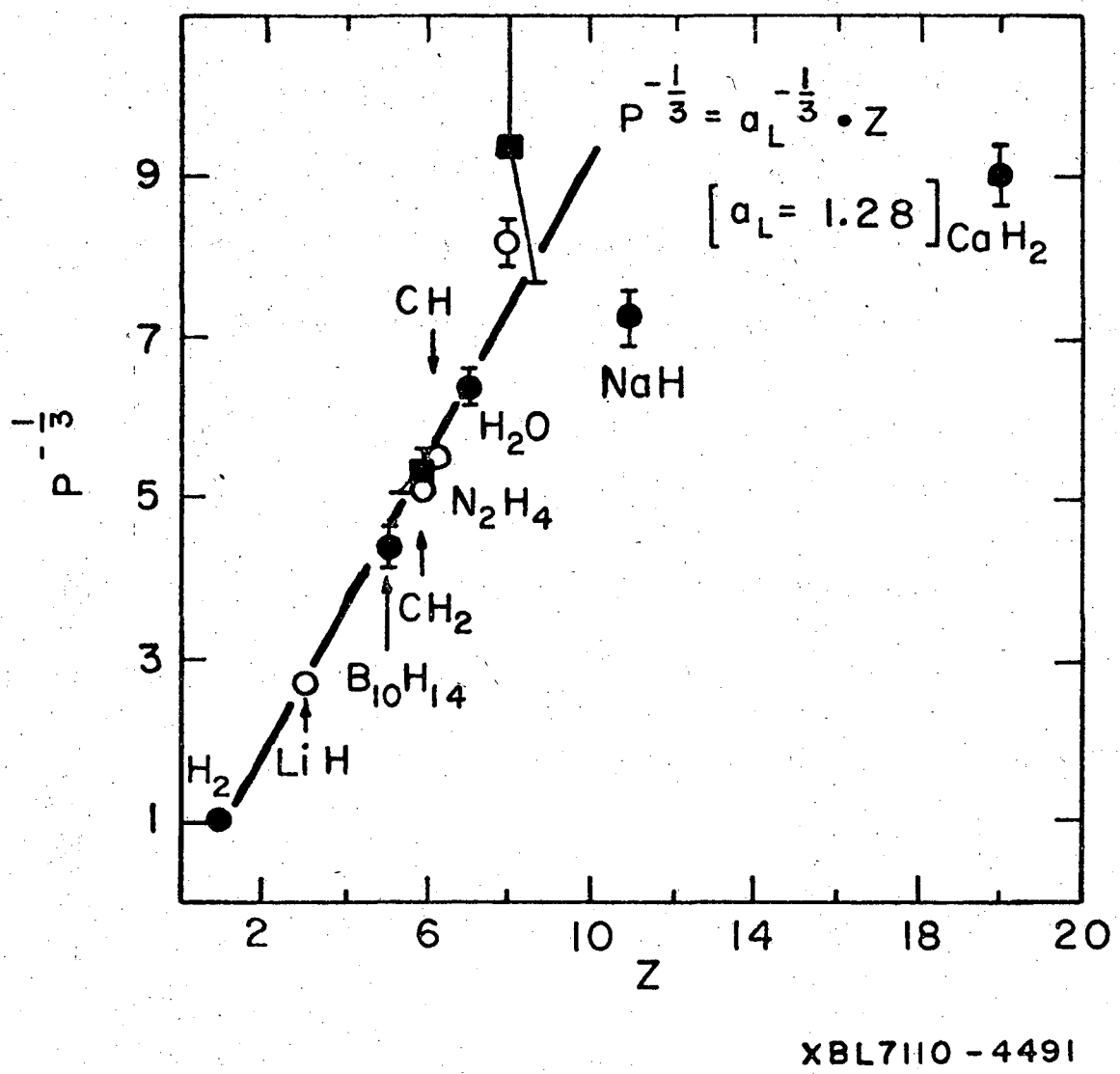

XBL7110-4491

Fig. 10

LEGAL NOTICE

This report was prepared as an account of work sponsored by the United States Government. Neither the United States nor the United States Atomic Energy Commission, nor any of their employees, nor any of their contractors, subcontractors, or their employees, makes any warranty, express or implied, or assumes any legal liability or responsibility for the accuracy, completeness or usefulness of any information, apparatus, product or process disclosed, or represents that its use would not infringe privately owned rights.

TECHNICAL INFORMATION DIVISION
LAWRENCE BERKELEY LABORATORY
UNIVERSITY OF CALIFORNIA
BERKELEY, CALIFORNIA 94720